*IOSR Journal of Applied Chemistry (IOSR-JAC)*
*e-ISSN: 2278-5736.Volume 13, Issue 2 Ser. I (February. 2020), PP 06-24*
*www.iosrjournals.org*

# Novel Schiff base ligand N-(6-chloropyrazin-2-yl)-4-{[(E)-(2-hydroxynaphthalen-1- yl)methylidene] amino} benzenesulfonamide (CPHNMABS), its metal(II) chelates and nanocomplexes: Synthesis, structural characterization, DNA, antitumor, docking studies, antimicrobial activity and conductivity studies.

Doaa F.Sallam[1], Tarek M.A. Ismail*[2], Abdel Razak M Tawfik[3] and Samy M. Abu-El-Wafa[4]
[1,2,3,4] Department of chemistry, Faculty of Education, Ain Shams University, Roxy, Cairo, Egypt.
*Corresponding Author:* Tarek M.A. Ismail

***Abstract:*** *A new series of solid Co(II), Ni(II), Cu(II) and Zn(II) chelates of the sulpha drug Schiff base ligand derived from condensation of sulphachloropyrazine and 2-hydroxy-1 naphthaldehyde were synthesized. The structures of the complexes were determined by Elemental and thermal analyses, $^{1}$HNMR IR, UV-Vis, ESR and Mass spectroscopy, molar conductance and magnetic studies. The obtaiend results show that the most metal (II) complexes are octahedral structures but few have square planer geometry. 3D modeling and the cluster calculations proved that the optimized (C=N)azomethine bond length elongated due to its coordination in I, IV, VII and X complexes. The Cu nanocomplexes were prepared in different media (EtOH, Cetyltrimethylammonium-bromide (CTAB), Malva Parviflora (MP) and Spinacia Oleracea (SO) and characterized by Transmission electron microscope (TEM) images and XRD pattern. The Cu nanocomplexes were tested as an antitumor agent towards Hepatocellular carcinoma cell line (HepG-2) and compared with cis-platin. The antitumor data revealed that the Cu nanocomplex (SO) XIV is more active than Cu nanocomplex (CTAB) XIII > cis-platin. The results of DNA cleavage studies showed that important role of Cu nanocomplex in isolated DNA cleavage reaction. The Cu nanocomplex (CTAB) XIII changed supercoiled DNA into open circular DNA. Therefore, it may be used as antitumor drugs in vivo to prevent the DNA replication in the tumor cells and to suppress the cancer for further increasing. Molecular docking studies of the free ligand and its Cu nanocomplex (EtOH) VII were reported and the results of this study have widened the scope of developing these sulphachloropyrazine compounds as promising antitumor drugs. Also, the antibacterial and antifungal activities towards ligand, its metal and its Cu nanocomplexes have been tested*

***Key Words:*** *Schiff base metal complexes, nano complexes, spectroscopic studies, antitumor activity, DNA cleavage, docking studies,*

---

Date of Submission: 29-01-2020 Date of Acceptance: 14-02-2020

---

## I. Introduction

Sulfonamides and its sulphachloropyrazine are the first drugs which played an important role as therapeutic agents against various diseases [1, 2]. Sulphachloropyrazine compound is largely used as antibacterial [3] antifungal [4] and antitumor [5, 6]. The Schiff base complexes derived from sulfa drugs have gained good complexing ability and biological activities [7-10]. There are many important applications for Cu nanoparticles; they act as semiconductor, an anti-biotic, anti-microbial, and anti-fungal agent [11, 12].

No literature found for Schiff base derived from sulphachloropyrazine, its metals and nanometal complexes, so our aim of study to throw more light on metal and nanocomplexes of sulphachloropyrazine with 2-hydroxy-1-naphthaldehyde. The prepared metal chelates are subjected to Elemental and thermal analyses, molar conductance, IR, Mass, $^{1}$HNMR, Electronic, ESR spectra and magnetic studies.

The electrical conductivity on the solid state for Cu nanocomplex (EtOH) VII and Cu nanocomplex (CTAB) XIII were measured. The synthesized ligand, its metal (II) chelates and its Cu nanocomplex for antimicrobial and antitumor activities have been tested.

## II. Experimental

### 2.1. Materials

The chemicals used were obtained from Aldrich, BDH or Merck products. The solvents used were methanol, ethanol, DMF and diethylether and were purified by the recommended methods [13].

### 2.2. The Apparatus and Physical Measurement

The apparatus and physical measurements used are present as previously mentioned in our puplications elsewhere [14, 15]

X-ray diffraction (XRD) patterns were obtained for the different solids, using a ″Brucker Axs D8″ Advance, Germany. The electrical conductivity was measured for both Cu nanocomplex (EtOH) VII and Cu nanocomplex (CTAB) XIII by using programmable automatic LCR Bridge (model RM6306 Phillips Bridge). The cluster calculations were performed by DMOL3 program [16] in Materials Studio program [17],

The anticancer activity of the investigated compounds was carried out against HepG2 cells (human Hepatocellular carcinoma) which gained from VACSERA Tissue Culture Unit according to literature technique [18, 19].

The DNA cleavage activity of Cu nanocomplexes was studied by using Agarose gel electrophoresis. The compounds were dissolved in DMSO and added separately to the CT-DNA (Calf Thymus DNA) .The sample mixtures were incubated at 37ºC for 1 hour. The electrophoresis of the samples was done using the following procedure. Weight 0.25gm of agarose and dissolve it in 25 ml of 1x TAE buffer by boiling. When the gel attains approximately 55ºC, pour it into the gel cassette fitted with comb. Let the gel to solidify. Remove carefully the comb, place the gel in the electrophoresis chamber flooded with TAE buffer. Carefully, Load DNA sample with bromophenol blue carefully into the wells, along with standard DNA marker with passing the constant 100 V of electricity untill the dye front reaches the end of gel. Carefully, Remove the gel and stain with ETBR solution (10 µg/ml) for 10-15 min and distain the gel with observatin the bands under UV trans illuminator of a gel documentation system (BIO-RAD, Gel Doc 2000) [20-21]. Molecular docking studies were carried using Molecular Operating Environment (MOE, 2015.10) software. All minimizations were performed with MOE till an RMSD gradient of 0.05 kcal·mol−1Å−1 with MMFF94x force field and the partial charges were calculated automatically. The X-ray crystallographic structure of carbonic anhydrase isoform II (CAII) co-crystalized with acetazolamide (PDB ID: 3HS4) was downloaded from the protein data bank. The prepared protein for the docking study using Protonate 3D protocol in MOE with default options. In order to define the binding site for docking, the co-crystalized ligand (acetazolamide) was used. Triangle Matcher placement method and London dG scoring function for docking have been used. The prepared compounds were tested for antimicrobial activity using disc-agar diffusion method.

### 2.3. Synthesis of Schiff Base Ligand

By mixing 1:1 molar ratio of an ethanolic solution from sulphachloro-pyrazine (2 gm, 0.007 mol) and 2-hydroxy-1-naphthaldehyde (1.2 gm, 0.007 mol) and refluxed for 8 hours. The formed yellow precipitate filtered off and recrystallized from ethanol then dried under vacuum to give yellow crystal, yield 95 %, m.p. 285 °C. Purity of the prepared ligand were tested by elemental analysis, IR, $^1$H NMR, UV-Vis and mass spectra Tables 1and 2

-$^1$H-NMR (300 MHz, DMSO-d6): 6.18 (s, 1H, NH exchangeable with D2O), 6.59 (d, 1H, J = 8.7 Hz, Ar-H), 7.24 (d, 1H, Ar-H), 7.30-7.604 (m, 4H, Ar-H), 7.79-7.84 (m, 2H, Ar-H), 8.04 (d, 1H, Ar-H), 8.89 (d, 1H, Ar-H), 8.26 (s, 1H, H-3pyrazine), 8.33 (s, 1H, H-5pyrazine), 8.95 (s, 1H, CH=N), 11.45 (s, 1H, OH exchangeable with D2O).

-UV-Vis spectra; λmax (nm), the band located at (275) assigned to π- π* transition of the aromatic system, the band within the (318) due to π- π* transition within the C=N groups. The band located at (447) assigned to an intermolecular charge transfer within the whole molecule (CT).

-Mass fragmentation spectrum of HL ligand under investigation is shown in Figure 1. The prepared Schiff base ligand fragmentation exhibits the molecular ion peak (m/e) = 438.5, as the same with its molecular weight. Scheme 1 showed the fragmentation of mass spectra of the ligand (CPHNMABS)

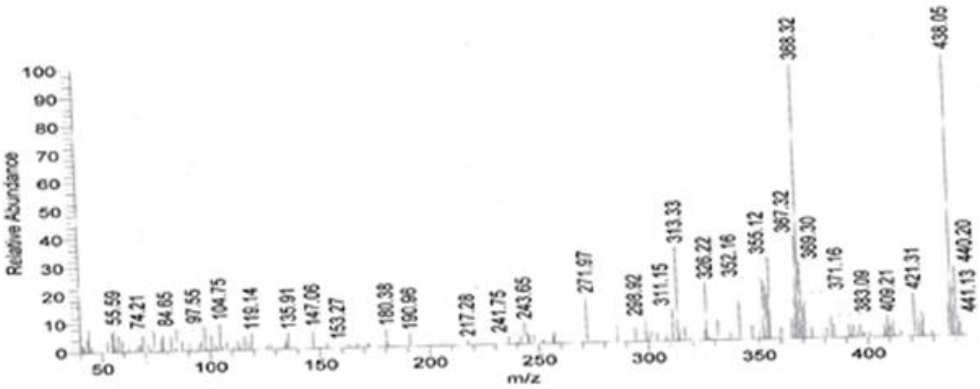


**Fig. 1**. Mass spectra of HL ligand

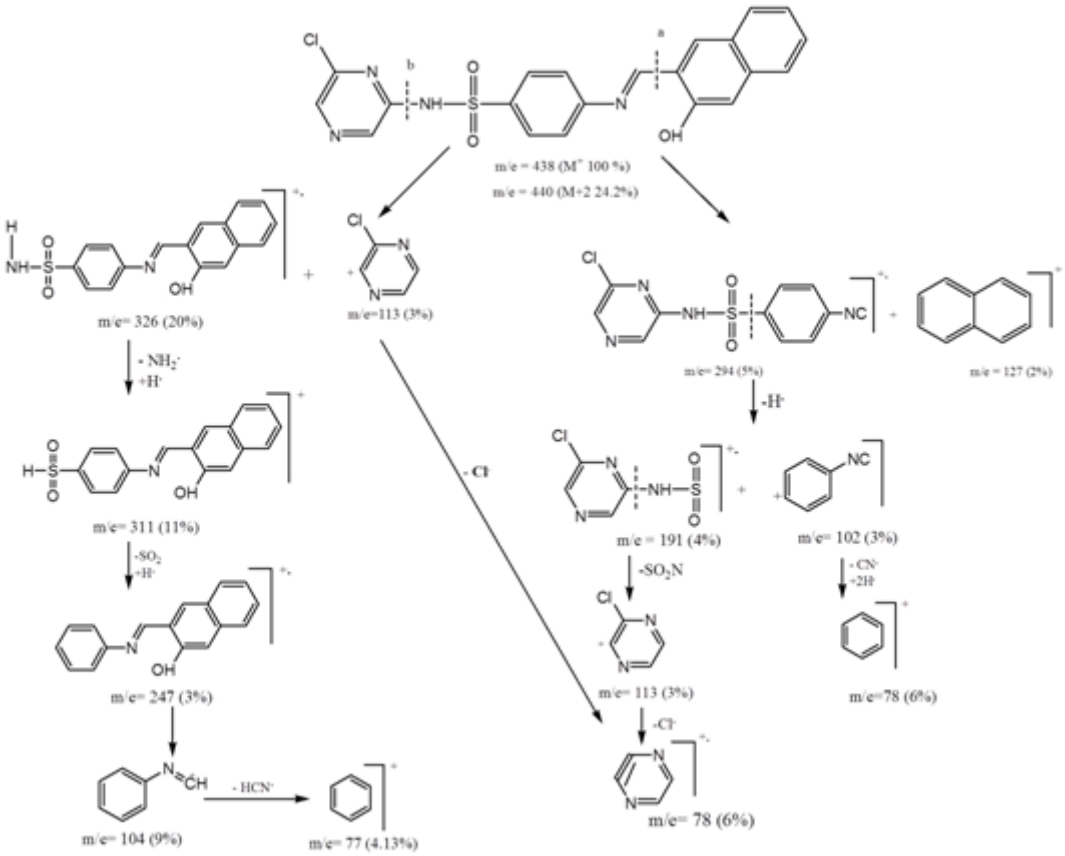


**Scheme 1** Mechanism of fragmentation pattern of Schiff base ligand (CPHNMABS).

The proposed structure of prepared ligand under investigation has the following structural formula, Figure2.

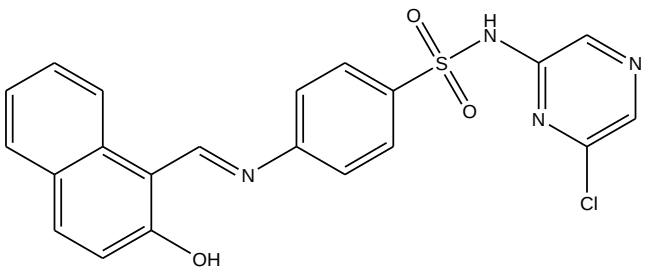

**Fig. 2** Schiff base ligand (HL)

N-(6-chloropyrazin-2-yl)-4-{[(E)-(2-hydroxynaphthalen-1-yl)methylidene] amino} benzenesulfonamide, CPHNMABS

**2.4. A. Preparation of the Solid Complexes**

The ehtanolic solution of Co(II), Ni(II), Cu(II) or Zn(II) nitrates were mixed with HL ligand dissolved in ethanol solution in a 2:1 (L:M) molar ratio. The resulting solutions are refluxed from 6 to 8 hours on a hot plate. The separated solid complexes are filtered off after cooling to room temperature, washed with small amounts of hot ethanol, bidistilled water, diethylether and eventually dried in vaccum desiccator over anhydrous CaCl2. All complexes are stabilized at room temperature, insoluble in popular organic solvents except DMF, nonhygroscopic.

**2.4. B. Preparation of Cu Nanocomplex**

Cu nanocomplexes XIII, XIV and XV were prepared according to Athwale et al [22] and by the method reported in [23, 24] using (CTAB) ,Malva Parviflora (MP) and Spinacia Oleracea (SO) extraction espectively. The nanostructure was characterized by TEM and X-ray diffraction (XRD) studies.

Transmission electron microscopy (TEM) picture of the Cu nanocomplex (EtOH) VII, Cu nanocomplex (CTAB) XIII, Cu nanocomplex (SO) XIV and Cu nanocomplex (MP) XV showed a small particle size in nanoscale range with a nano feature products, Figures 3and4. The particles size of nano complexes VII , XIII, XIV and XV have 15 nm , 4.4 nm 45 nm and 33 nm respictevly.

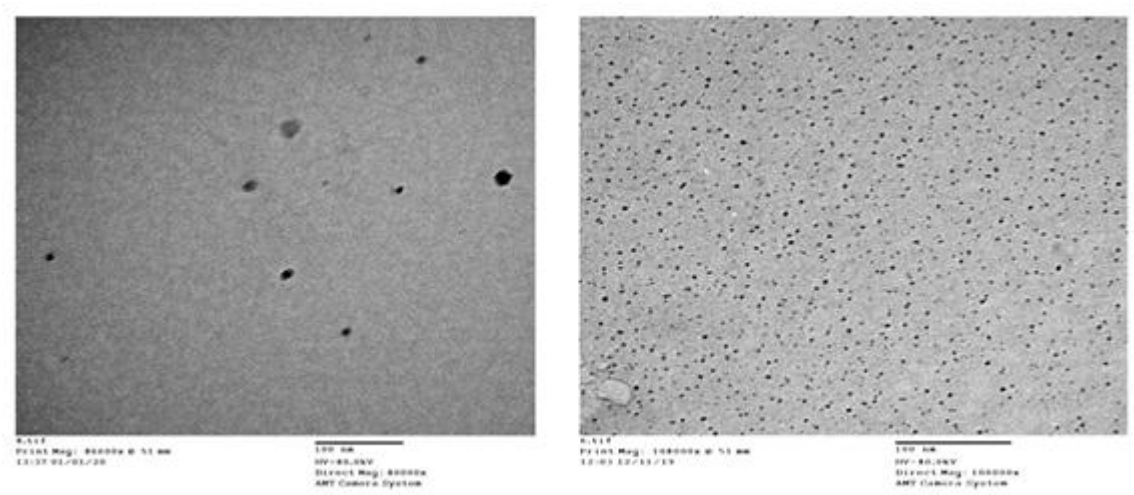

**Fig.3** TEM images of Cu nanocomplexes VII and XIII.

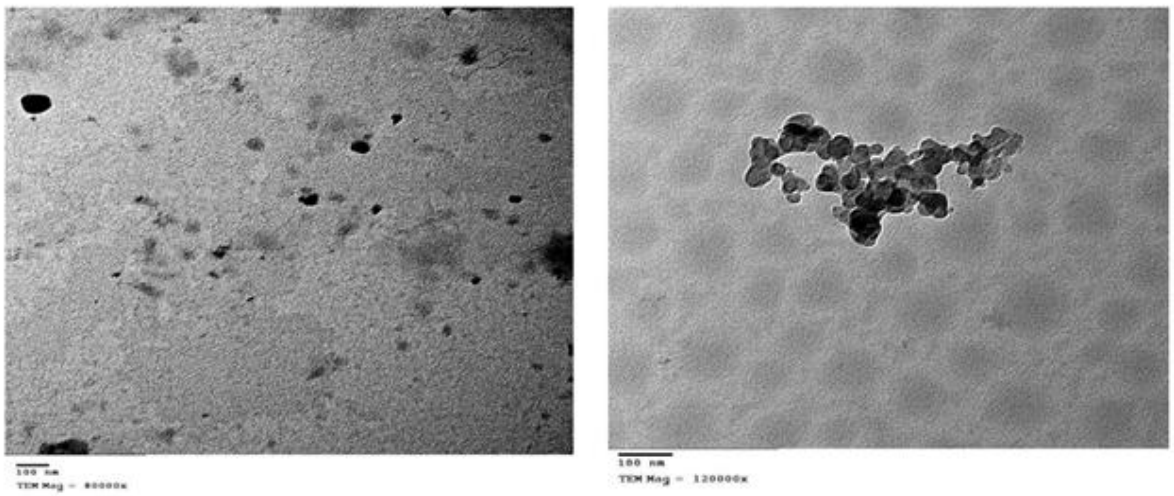

**Fig. 4** TEM image of Cu nanocomplex of XIV and XV.

The powder X-ray diffraction studies were carried out for Cu nanocomplexes Figure 5. The Cu nanocomplexes XIII, XIV and XV are amorphous in nature, while the diffraction patterns showed crystalline in nature of Cu

nanocomplex VII. The average crystal sizes of nanocomplexes were calculated by using Debye Scherrer equation [25].
The Cu nanocomplex VII and XIII have a crystalline size of 28nm and 18 nm respectively suggesting that the complexes are in a nanocrystalline phase [26].

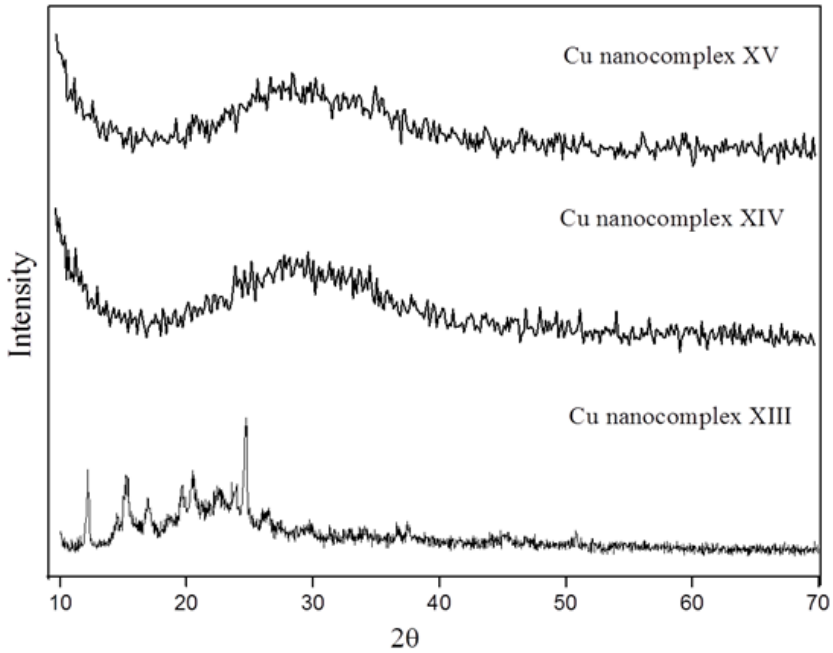


**Fig. 5** Powder XRD patterns of the Cu nanocomplexes XIII, XIV and XV.

### 2.6. Preparation of Mixed Ligand Complexes

The procedure of prepared solid mixed complexes II, III, V, VI, VIII, IX, XI and XIII were obtained by the method discussed elsewhere [14 ,15 ].

## III. Result And Discussion

### 3.1. Elemental Analysis and Molar Conductance of Solid Complexes

Elemental analysis and molar conductance have been carried out and listed in Table 1. The analytical data of the prepared complexes are in good agreement with the proposed structures. The result of elemental analysis of the synthesized complexes revealed that the metal ions reacted with the ligand in molar ratios 1: 2 (metal: ligand) for complexes I, IV, VII and X. The results indicated that the ligand acts as bidentate towards the metal ions via the azomethine –N atom and phenolic –O atom. The chemical composition of the mixed ligand complexes under investigation (CPHNMABS) and 1, 10 Phenanthroline (1,10 phen) or 8-hydroxyquinoline (8-HQ) with Co(II), Ni(II), Cu(II) and Zn(II) ions are determined from the elemental analysis results which listed in Table1. The results of the elemental analysis indicated that the metal ions reacted with the ligand (CPHNMABS) and 1, 10 Phenanthroline or 8- hydroxy-quinoline (8-HQ) in the molar ratios 1: 1: 1 (M: L: 1, 10 phen or 8-HQ) for the complexes II, III, V, VI, VIII, IX, XI and XII.

The elemental analysis data revealed that the Schiff base ligand (CPHNMABS) acta as bidentate ligand towards metal ion through azomethine nitrogen atom and phenolic oxygen atom.

The results revealed that most of the prepared complexes have one or more $H_2O$ or EtOH molecule associated with the complex which are not removed by static vaccum for seven hours at room temperature. The molar conductance values ($\Omega$ ohm$^{-1}$ cm$^2$ Mol$^{-1}$) of the metal complexes was collected in Table 1. All solid complexes have $\Omega_m$ values within the range (4.0-15.93 ohm$^{-1}$ cm$^2$ mol$^{-1}$) revealed the non-electrolytic behavior of complexes, so that all these complexes are neutral [27].

### 3.2. IR Spectral Studies

On comparing the IR spectra of the schiff base ligand under investigation with those of prepared metal (II) complexes Table 2, the following can be pointed out.
i. The IR spectra of most solid complexes exhibit a broad band within the range 3453- 3424 cm$^{-1}$, which is attributed to the υOH of water and/or EtOH molecules associated with the complex. The existence of the new bands at 625- 694 cm$^{-1}$ for complexes II, III, IV, V, VI, VII, X and XII is attributed to p$H_2O$ of coordinated water molecules, indicating the presence of coordinated water molecules in the metal ion complexes.

ii. The disappearance of υOH phenolic in the IR spectra of all solid complexes under investigation which are observed at 3415 $cm^{-1}$ in the IR of the free ligand, showed that proton displacement from the phenolic υOH group takes through the metal ion. This is confirmed by the existence of new bands at 504- 586 $cm^{-1}$ in the IR spectra of all metal chelates which are absent in the IR spectra of the free ligand which could be assigned to υM-O bonds [28].
iii. The υC=N band observed at 1629 $cm^{-1}$ in the IR of the free ligand is shifted to lower wave numbers by 7-20 $cm^{-1}$ in the IR spectra of all metal complexes under investigation, denotes that the coordination of the azomethine nitrogen atoms to the metal ions, which is supported by the existence of new bands in the IR spectra of all metal complexes at 409- 466 $cm^{-1}$, these bands would be assigned to υM-N bonds [29].
iv. The complexes II, V, VIII and XI show new bands at 1384 - 1385 $cm^{-1}$ due to $NO_3^-$ ion which supports the coordinated nature of the $NO_3^-$ ion through nitrogen atom [30].
v. The IR spectra of Schiff base ligand has two characteristic bands of $\upsilon(SO_2)_{asm.}$ at 1154$cm^{-1}$ and $\upsilon(SO_2)_{sym.}$ at 1093 $cm^{-1}$ These bands appear also at the same position in case of all solid complexes under investigation indicating that the $SO_2$ group does not coordinated to metal ion.

### 3.3. $^1$H-NMR Spectral Studies

On comparing of the $^1$HNMR spectra of the ligand (CPHNMABS) and its Zn (II) complex (X) recorded in DMSO-d6 Table 3, the following can be pointed out
i. The signal at δ (8.95) (s, 1H) due to the azomethine proton (-N=CH-) of the Schiff base (HL) shifted downfield in the region of δ (9.18) (s, 1H), supporting the coordination of the nitrogen of the (-N=CH-) group with the metal ion.
ii. The peak due to phenolic OH proton originally present at δ 11.95 ppm in free Schiff base ligand (CPHNMABS) is completely absent from the spectra of Zn(II) complex indicating the bonding through phenolic oxygen atom.

### 3.4. Thermal Studies

TGA (Thermal gravimetric analysis) is used to throw some light on the thermal stability of the investigated complexes and to define whether the solvent or water molecules are inside or outside the coordination sphere [31, 32].
The Cu nanocomplex (CTAB) XIII was subjected to thermal heat at 650$^o$C and the resultant compound after heating was analysed by TEM the particle size is increased over thermal heating from 4.4 nm (subnano) to 57 nm, Figure 6.

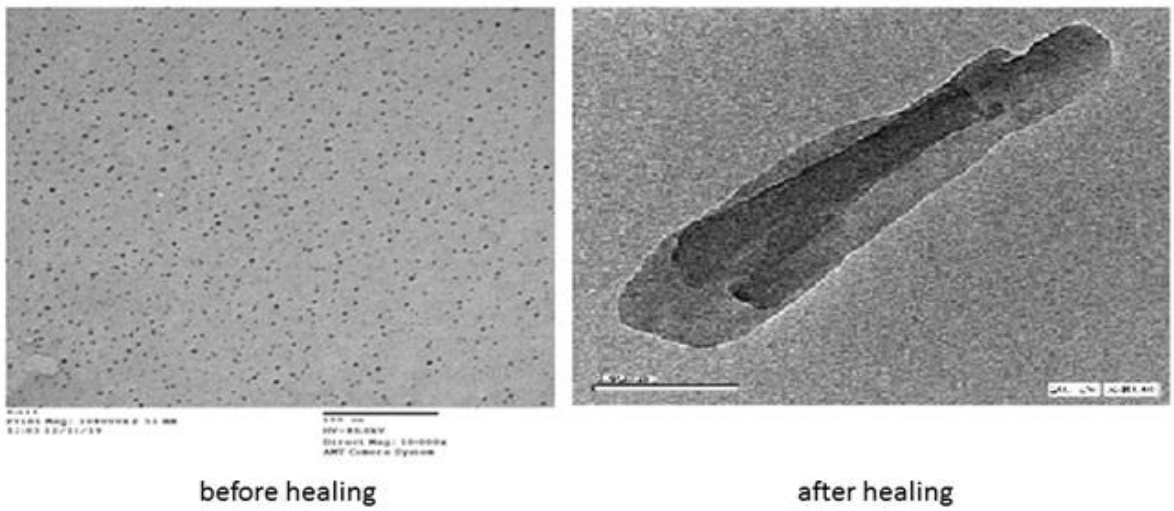


**Fig. 6** TEM image of Cu nanocomplex XIII after heating at 650$^o$C.

Figure 7 shows the TGA- DTGA curves for complexes I, IV and VII.
For the Co(II) complex, a mass loss occurred within the temperature range 34-96˚C corresponding to the loss of 20.8% (Calcd 21.4%) for two molecules of coordinated ethanol and two $SO_2$ molecules . At the temperature range 96.6-365 ˚C another loss of 25.62% (Calcd.25%) for $C_8H_6N_6Cl_2$ as apart of ligand decomposition. In the temperature range 365-400 ˚C a mass loss of 9.29% (Calcd. 10.03%) as another part of the copmpound. At higher temperature range 400.6 - 799 ˚C a loss of 35.8% (Calcd. 36.1%) corresponding to $C_{27}H_{17}NO$ as another part of the compound, then it forms CoO.

For the Ni (II) complex, a mass loss occurred within the temperature range 34 – 110 ˚C, corresponding to the loss of 4.38% (calcd.5.27%) for three lattice water molecules and at the temperature range 110 – 393˚C, another loss of 24.87% (calc.25.5%) for another two coordinate water, $2SO_2$, $Cl_2$ and one molecule of HCN. At higher temperature range 393.5 - 735 ˚C a loss of 62.4% (Calcd. 61.84%) corresponding to $C_{41}H_{27}N_7O$ decomposition of the compound then it gives NiO.
For the Cu (II) complex, a mass loss occurred within the temperature range 38.5 – 120˚C corresponding to the loss of 5.7 % (Calcd.6.08%) for four molecules of lattice water. At the temperature range 122– 340.8˚C another loss of 26.78% (Calc.27.6) % for two coordinated water molecules, $2SO_2$, $Cl_2$ and 2HCN. At higher temperature range 341.3 – 796.5˚C a loss of 58.6% (57.9%) corresponding to $C_{40}H_{26}N_6O$ from the compound, then it forms CuO.
The order, n and activation energy, E* of the decomposition steps for Co(II), Ni(II) and Cu (II) complexes are determined from TGA results by using the Coats-Redfern equation [33], the thermo kinetic parameters are calculated and collected in table 4.
From the obtained data the following remarks can be pointed out:
i. The ΔS* has a positive value for all the metal complexes. This revealed that the activated complex is less ordered than the reactants and / or the reactions are fast [34].
ii. The positive value of ΔG* indicated that the free energy of the final residue is higher than that of the initial compound. This means that all the the steps of decomposition are nonspontaneous [35].
iii. The activation enthalpy change has a positive values ΔH* revealed that the stages of decomposition are endothermic.

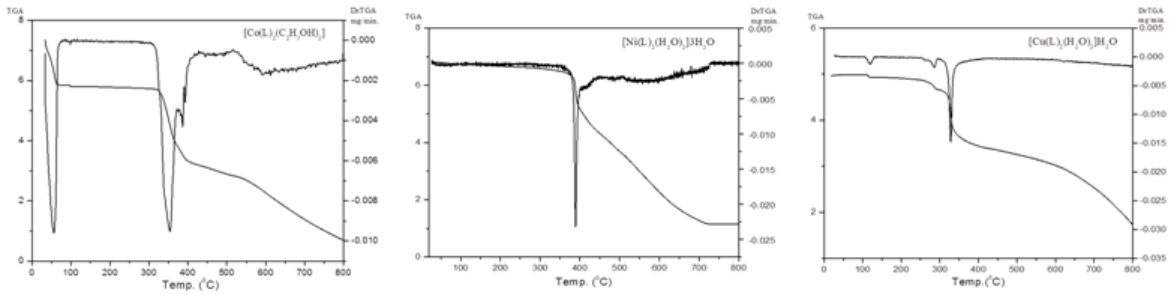


**Fig. 7** TGA - DrTGA curves of complexes I, IV and VII.

Nanocomplex XIII shows two S shape steps whereas complex XIV and XV show one S shape step. The thermal stability of Cu nanocomplex XIII indicates thermal stability up to 300$^o$C. After this temperature some rearrangement increase in particle size from subnano 4.4 nm to nanoparticle 57 nm, while nanocomplex XIV( particle size 45nm) and XV( particle size 33nm) have thermal stability up to 200$^o$C, Figure 8. Above this temperature some rearrangement in particle sizes are increased at temperature 400$^o$C for complex XIV and temperature 650$^o$C for complex XV.

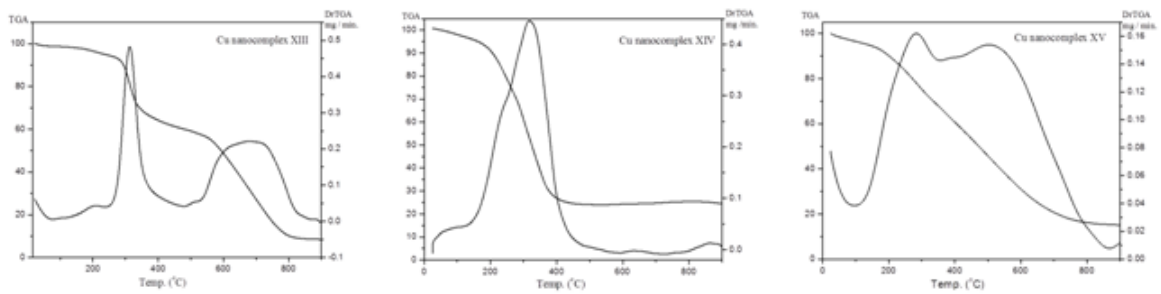


**Fig. 8** TGA - DrTGA curves of Cu nancomplexes XIII, XIV and XV.

The TG analyses suggest higer thermal stability for nano complexes than metal (II) complexes so these nano Cu complexes may be applied in industry as a ceramic coating [ 36].
From the decomposition temperatures of metal (II) complexes the thermal stability was deduced in the order
Complex VII > Complex IV > Complexe I
Also, the thermal stability of Cu nanocmplexes XIII, XIV and XV was deduced in the order
Cu nanocomplex XIV > Cu nanocomplex XV > Cu nanocomplex XIII.

**3.5. Magnetic Properties**

The magnetic moment values are obtained at room temperature which listed in Table 3. The magnetic measurements for all Co (II) and Ni(II) complexes showed magnetic moment values of 4.97 - 5.01 and 3.1 - 4.2 BM respectively, indicating consistency with their octahedral environment [27]. The Cu(II) complexes VII , VIII and IX showed the magnetic moment values of 2.06 , 2.07 and 1.8 BM respectively expected for one unpaired electron, which refer to the possibility of a distorted octahedral [37, 38].

**3.6. Electronic Spectral Studies**

The electronic spectra of the complexes (I – IX] are recorded in freshly prepared DMF solution ($10^{-3}$ M) at room temperature and the spectral data are reported in Table 4. The electronic absorption spectra of the Co(II) complexes namely I, II and III show bands at 579, 589 and 582 nm respectively corresponding to $^{4}T_{1g}(F) \rightarrow {}^{4}A_{2g}(P)$ and $^{4}T_{1g}(F) \rightarrow {}^{4}T_{1g}(P)$ transitions indicating octahedral structure[39].

The Ni(II) complexes IV, V , VI exhibited two absorption bands, at 545 - 646 and 729 - 759 nm ranges respictively, assignable to $^{3}A_{2g}(F) \rightarrow {}^{3}T_{1g}(F)$ and $^{3}A_{2g}(F) \rightarrow {}^{3}T_{1g}(P)$ transitions,respectively, in an octahedral environment [40].

The Cu(II) complexes VII, VIII and IX have a single broad asymmetric band in the region of 542 - 715 nm ranges corresponding to $^{2}Eg \rightarrow {}^{2}T_{2g}$ transitions. The broadness of the band due to dynamic Jahn-Teller distortion. All of these data suggested a distorted octahedral geometry around the Cu(II) ion in all the complexes [41].

The electronic spectra of the Zn(II) complexes do not furnish any relevant data towards stereochemistry as expected, but from analytical, conductance, and IR spectral results, square planner structure is proposed for the complex XII while the complexes X and XI have octahedral geometries.

The electronic spectra Cu nanocomplex (CTAB) XIII shows two peaks at 616 and 674 nm, Cu nanocomplex (SO) XIV shows peak at 648 and Cu nanocomplex (MP) XV shows two peaks at 600 and 650 nm which differ from the absorption spectrum peak of Cu(II) complexes.

**3.7. ESR Spectra of Cu (II) Complexes**

X-band ESR spectra of Cu(II) complexes namely VII, VIII and IX are recorded at room temperature as shown in Figure 9. The geff values of Cu(II) complexes are collected in Table 5. From $g_{eff}$ values and shape of ESR signals, the investigated Cu(II) complexes suggested to have distorted octahedral geometry.

From the observed g-values of the Cu (II) complexes, it is clear that $g_{\parallel} > g_{\perp}$ which indicated that the unpaired electron in the $dx^2$-$y^2$ orbital is predominantly [42] giving $^{2}B_{1g}$ as the ground state. The observed data showed that the $g\parallel$ values are > 2.0023 for complexes. This reveals that the metal-ligand bonding in these metal complexes is covalent character [43]. The g-values related by this expression, $G = (g\parallel - 2) / (g\perp - 2) = 4$, which measure the exchange interaction between the Cu(II) centers in the solid. If G value is higher than 4, the exchange interaction between the Cu(II) centers is negligible, while G is lower than 4 a considerable exchange interaction is showed in the solid complex. The calculated G values for complexes VII, VIII and IX are 1.23, 1.16 and 1.13 respectively which proposed a Cu-Cu exchange interaction [44]

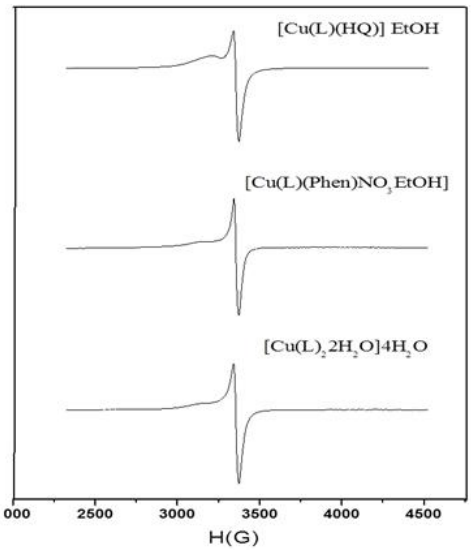


**Fig. 9** X-band ESR spectra of Cu (II) complexes.Table 5

## IV. Theoretical studies of ligand and its metal complexes

The geometrical structures of the prepared ligand and its metal complexes X, IV, VII and I are optimized. Molecular modeling of free ligand HL and its Cu(II) complex shown in Figures 10,11 respectively.

-The LUMO - HOMO energy gap (ΔE) is an important approach to study the stability of metal complexes. While the LUMO – HOMO energy gap decreases, the interactions between the reacting species will be stronger and lead to increase the stability of the formed metal complexes [45]. The values of ΔE showed that the ligand under study have high inclination to bind with the metal ions [46]

- The order of Egap (eV) that measures the reactivity of the Schiff base ligand and its metal complexes is: X > IV > VII > I > free ligand HL, Figures 12 and 13.

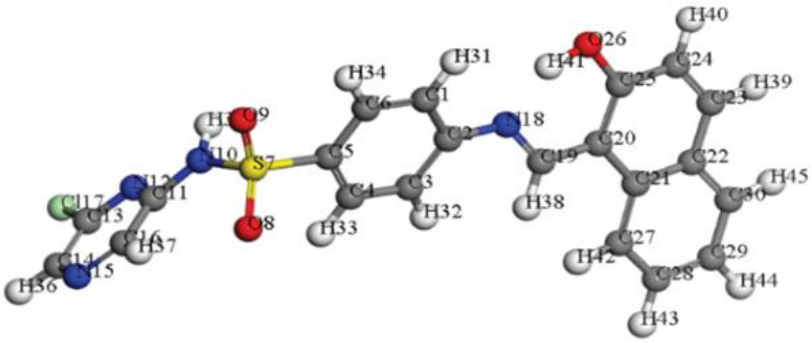

**Fig. 10** Molecular modeling of Schiff base ligand HL.

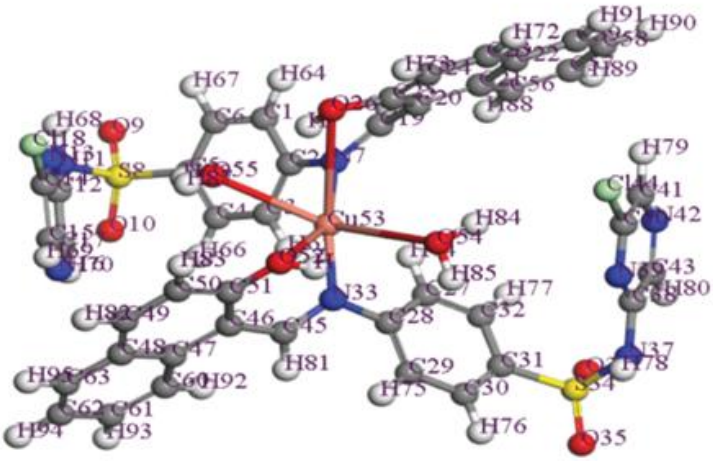

**Fig. 11** Molecular modeling of $Cu^{+2}$ complex.

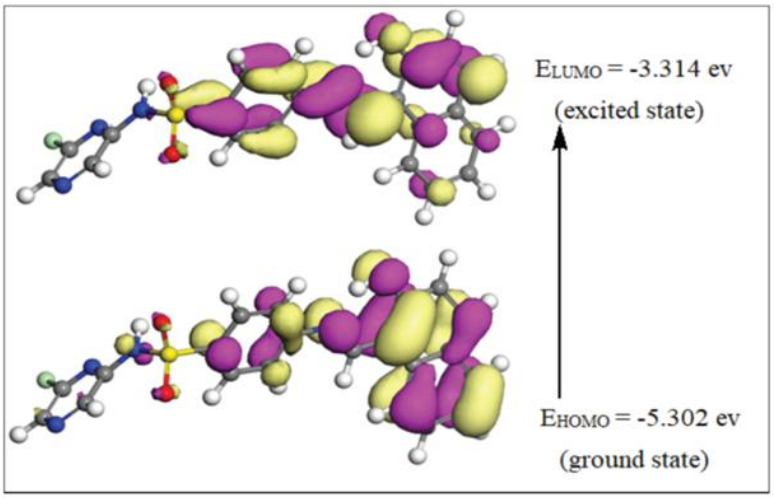


**Fig. 12** 3D plots frontier orbital energies using DFT method for HL ligand.

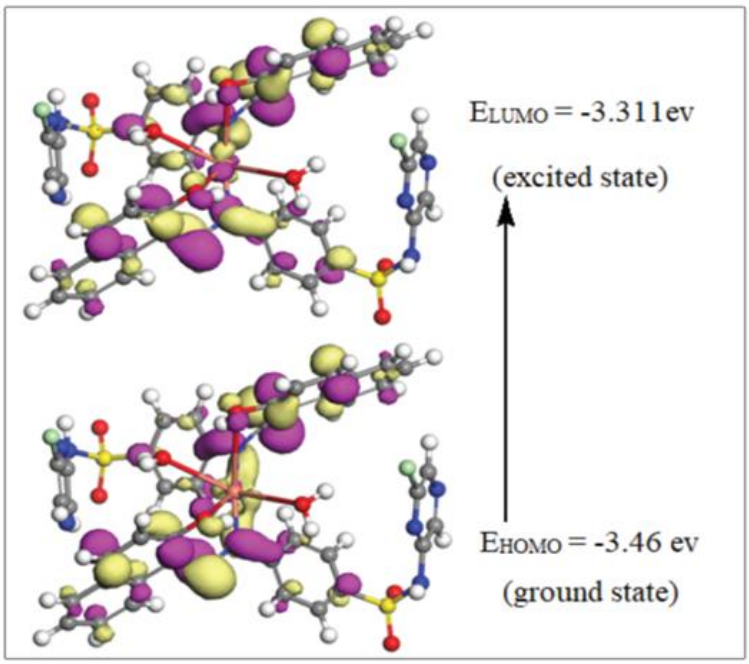


**Fig. 13** 3D plots frontier orbital energies using DFT method for Cu+2complex.

**4.1. Bond Lenhgth and Bond angle**

Analysis of the data of bond lengths was calculated in Table 7. The obtained results show the following remarks:

1. The optimized $(C{=}N)_{azomethine}$ bond length elongated due to its coordination in I, IV, VII and X complexes.
2. The N(33) - C(45)azomethene, C(51) - $O(52)_{phenolic}$ bond lengths becomes slightly longer in complexes as the coordination takes place via N(33) of azomethene group and O(52) atom that is formed on deprotonation of OH phenolic group.
3. There is elongation in C(51) – O(52) bond distance in all metal(II) complexes due to the formation of the M-O bond which cause weakness in C – O bond [47].
4. The bond angles of Schiff base ligand are changed somewhat upon coordination; the largest change affects O(26)-C(25)-C(20) and C(20)-C(19)-N(19) angles which are increased or reduced on complex formation as a consequence of bonding [47].
5. The bond angles in I, IV, and X complexes lie in the range reported for octahedral geometry and distorted octahedral in case of complex VII predicting $SP^3d^2$ or $d^2SP^3$ hybridization.
6. The bond angles within the sulphachloropyrazine moiety do not change but the angles around the metal ion changed as a result of coordination with the ligand.

## V. Biological Activities

**5.1. Antitumor activity**

Schiff base ligand (CPHNMABS) and its Cu nanocomplexes VII ,XIII and XIV are tested as an antitumor agent towards Hepatocellular carcinoma cell line (HepG-2) with cis-platin. As shown in Figure 14. IC50 values were calculated and the results were collected in Table 8.

$IC_{50}$ means that the inhibition concentration of a substance that inhibit 50% of the tumor cell**.** The obtained results show that Cu nanocomplex VII is more active than free ligand. This indicated the enhancement of antitumor activity upon coordination. Both Cu nanocomplexes XIV with $IC_{50}$ value of 2.46 µg/ml and XIII with $IC_{50}$ value 3.5 µg/ml show high antitumor activity, this nanocharacter increased the antitumor activity due to easily penetration of Cu nanocomplex into cancer cell.The antitumor activity resultes show nanocomplex XIV is the highest cytotoxicity compound.

The order of antitumor activity is Cu nanocomplex XIV > Cu nanocomplex XIII > Cu nanocomplex VII > Schiff base ligand.

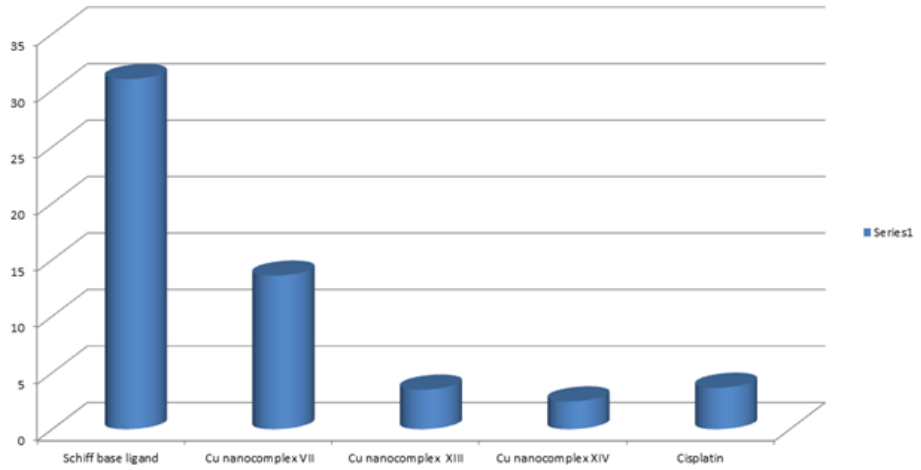


**Fig. 14** In vitro antitumor activities of Schiff base ligand and its Cu nanocomplexes on Hepatocellular carcinoma cell line (HepG-2).

**5.2. DNA cleavage studies**

DNA cleavage is performed by using gel electrophoresis experiment on the Cu nanocomplex VII and Cu nanocomplex XIII. Figure 15 showed the effect of fixed concentration of complexes on different concentration of DNA; the pattern of DNA binding of the agarose gel electrophoresis diagram showing lane L-marker 1kb DNA Ladder, lane (1) DNA control, lane (2) DNA+DMSO, lane (3) 200ng DNA+ 0.5mg\ml Cu nanocomplex VII, lane(4) 400ng DNA+0.5 mg\ml Cu nanocomplex VII, lane (5) 600ng DNA+0.5 mg\ml Cu nanocomplex VII, lane (6) 200ng DNA+0.5 mg\ml Cu nanocomplex XIII, lane (7) 400ng DNA+0.5 mg\ml Cu nanocomplex XIII , lane(8) 600 ng DNA+0.5 mg\ml Cu nonocomplex XIII.

Figure 16 indicated that the effect of different low concentrations of complexes on DNA; the pattern of DNA of the agarose gel electrophoresis diagram showing lane L- marker 1kb DNA Ladder, lane (1) DNA control , lane (2) DNA+DMSO, lane (3) 400ng DNA+1mg\ml Cu nanocomplex VII, lane (4) 400ng DNA+2.5mg\ml Cu nanocomplex VII, lane (5) 400ng DNA+4mg\ml Cu nanocomplex VII, lane (6) 400ng DNA+1mg\ml Cu nanocomplex XIII, lane (7) 400ng DNA+2.5mg\ml Cu nanocomplex XIII, lane (8) 400 ng DNA+4mg\ml Cu nanocomplex XIII.

Figure 17 showed effect of different high concentrations of complexes on DNA; the pattern of DNA of the agarose gel electrophoresis diagram showing lane L- marker 1kb DNA Ladder, lane (1) DNA control, lane(2) DNA+DMSO, lane (3) 400ng DNA+5mg\ml Cu nanocomplex VII, lane (4) 400ng DNA+ 10mg\ml Cu nanocomplex VII, lane (5) 400ng DNA+15 mg\ml Cu nanocomplexVII, lane (6) 400ng DNA+5 mg\ml Cu nanocomplex XIII, lane(7) 400ng DNA+ 10 mg\ml Cu nanocomplex XIII, lane (8) 400 ng DNA+ 15 mg\ml Cu nanocomplex XIII.

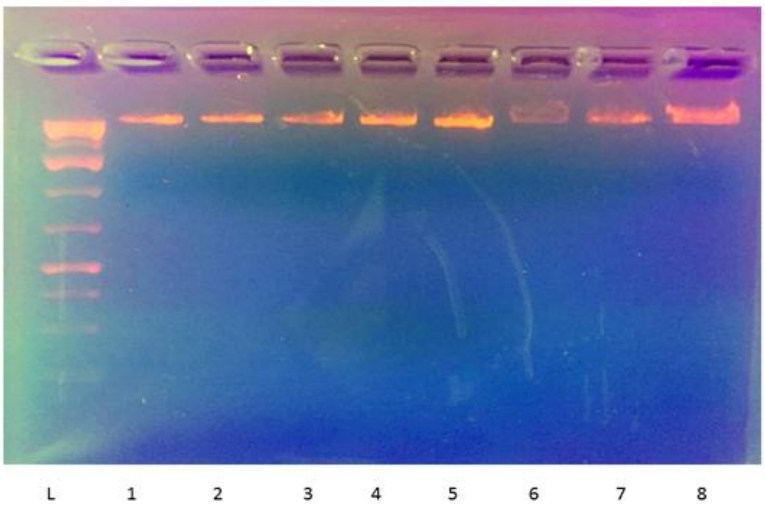


**Fig. 15** Effect of fixed concentration of complexes on different concentration of DNA.

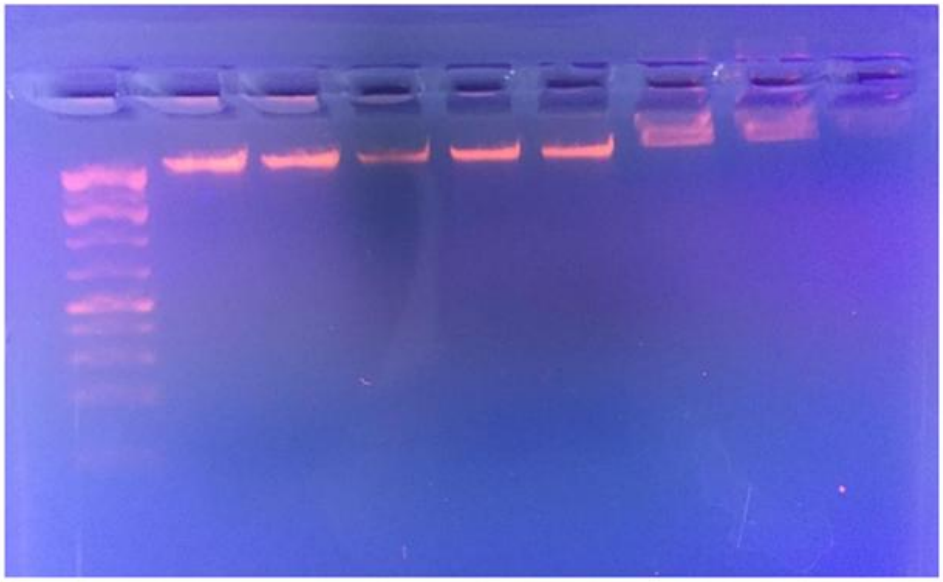

L 1 2 3 4 5 6 7 8

**Fig. 16** Effect of different low concentrations of complexes on DNA.

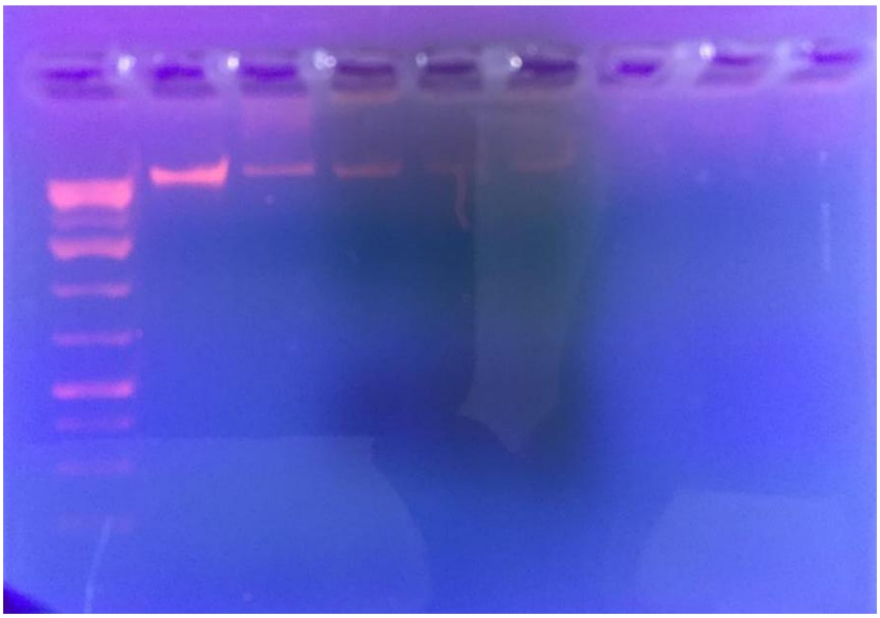

L 1 2 3 4 5 6 7 8

**Fig. 17** Effect of different high concentrations of complexes on DNA.

The two investigated Cu nanocomplex VII and Cu nanocomplex XIII were tested to study their effect on DNA; Cu nanocomplex VII has no ability to cleavage DNA even with different concentration of DNA or when used fixed concentration of DNA with different concentration of Cu nanocomplex VII Figures (15 - 17) While, Cu nanocomplex XIII has only the ability to cleavage DNA at low concentration (1, 2.5 and 4 ug) Figure 16. However, at high concentration (5, 10 and 15 ug) has severe effect on DNA; it could be destroying DNA Figure 17. The results reveal that important role of Cu nanocomplex XIII in isolated DNA cleavage reaction. The Cu nanocomplex XIII can be converted supercoiled DNA into open circular DNA. Therefore, The Cu nanocomplex XIII can be used as antitumor drugs in vivo to prevent the DNA replication in the tumor cells and to suppress the cancer for further increasing.

**5. 3. The molecular docking**

Docking setup was first validated by self-docking of the co-crystallized ligand (acetazolamide) in the vicinity of the binding site of the enzyme**,** Figure 18. The molecular docking studies of the prepared Schiff base ligand (CPHNMABS) and its Cu complex VII were carried out and the results are summarized , Figure 19 and Table 9.

The validated setup was then used for predicting the ligand-receptor interactions at the binding site for the compounds of interest. The ability of the target compounds to interact with the key amino acids & $Zn^{+2}$ in the binding site rationalizes their good activity as indicated by their docking pattern and docking scores compared to that of acetazolamide.

The docking study showed that metal complex is potential inhibitors of cancer causing receptors. This study has widened the scope of developing these sulphaclozine compounds as promising antitumor drugs

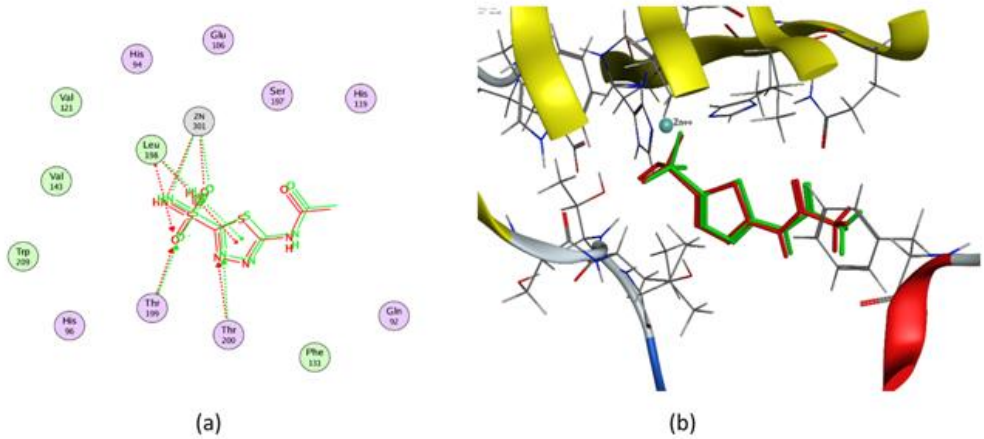


**Fig. 18** (a) 2D representation and (b) 3D representation of the superimposition of the co-crystallized (red) and the docking pose (green) of acetazolamide in CAII binding site with RMSD of 0.2981 A°.

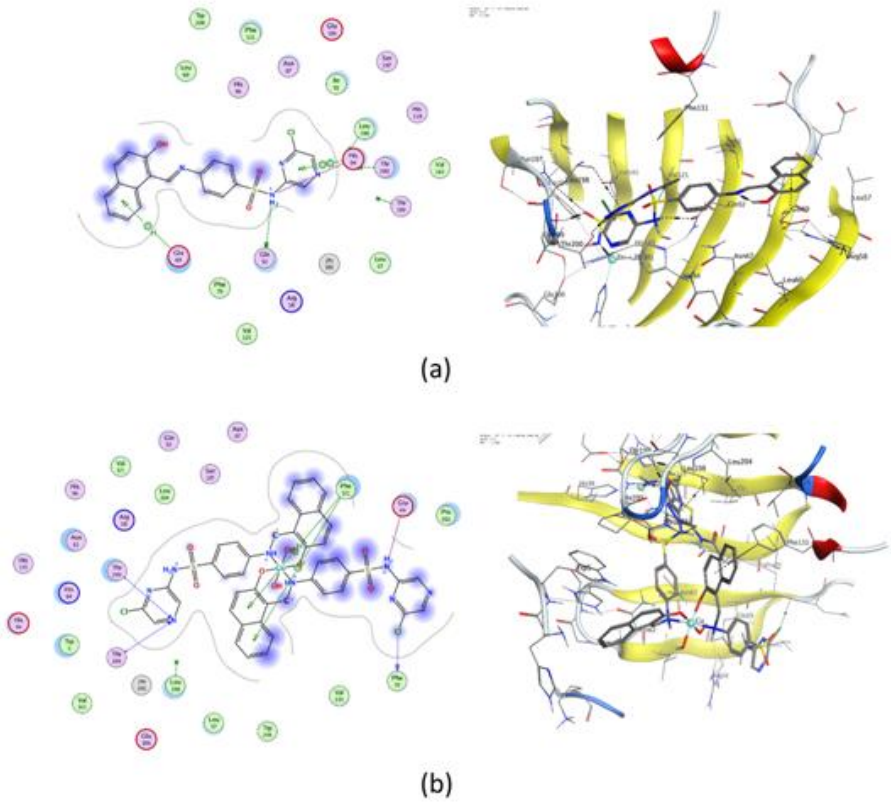


**Fig. 19** 2D & 3D diagrams of Schiff base ligand (a) and of Cu(II) nanocomplex (b) VII showing its interaction with the CAII binding site.

**5.4. Antibacterial and Antifungal Assays**

The biological activities of prepared ligand, its complexes ( I and IV) and Cu nanocomplexes (VII , XIII, XIV and XV) are screened for their antibacterial and antifungal properties by the agar diffusion method in DMF solvent against *Escherichia coli*, *Bacillus subtilis*and *Salmonella typhi* bacteria, *Staphylococcus aureus, Candidaalbicans* and *Aspergillus fumigatus* fungi. The results of antifungal activity and antibacterial of tested ligand and its complexes are collected in Table 10 and Figure 20.

A comparative study of the free ligand (CPHNMABS) and its complexes showed that most complexes have higher antimicrobial activity than the free ligand. The higher activity of the complexes was explained using of Tweedy's chelation theory [48] and Overtone's concept [49]. All these metal complexes also disturb the respiration process of the cell and hence blocked the synthesis of the proteins and restricting the growth of the organism. Addition to, the formation of a hydrogen bond through the azomethine group with the active center of the cell, leading to interference with the normal cell processes. In general, metal complexes are more active than free ligand (CPHNMABS) due to these complexes may act as a vehicle for the activation of ligand as the principle cytotoxic species [50]. Cu nanocomplex XIII showed higher antimicrobial activity than the free ligand and its metal chelates, this is because of its high surface to volume ratio are very reactive which can interact with other particles easily and increase its antimicrobial efficiency [51].

This difference in activities is related also to the complex formation between free HL ligand and Cu nanoparticles, leading to super strong materials which increase its antimicrobial efficiency. The prepared complexes have a variety of antimicrobial activities towards all microorganisms.

Ni(II) complex IV has higher activity towards *Bacillus subtilis* and *Salmonella typhimurium* than other complexes while Cu nanocomplex VII has higher activity toward *Staphylococcus aureus* and *Candida albicans than other complexes.*

Co (II) complex I showed good activity towards Aspergillus *fumigates.*

Generally, the antimicrobial activity orders are:

Cu nanocomplex XV > Cu nanocomplex XIII > Cu nanocomplex XIV> Ni(II) complex IV > Cu(II) nanocomplex VII > Co(II) complex I > free ligand as shown in the Fig. 8

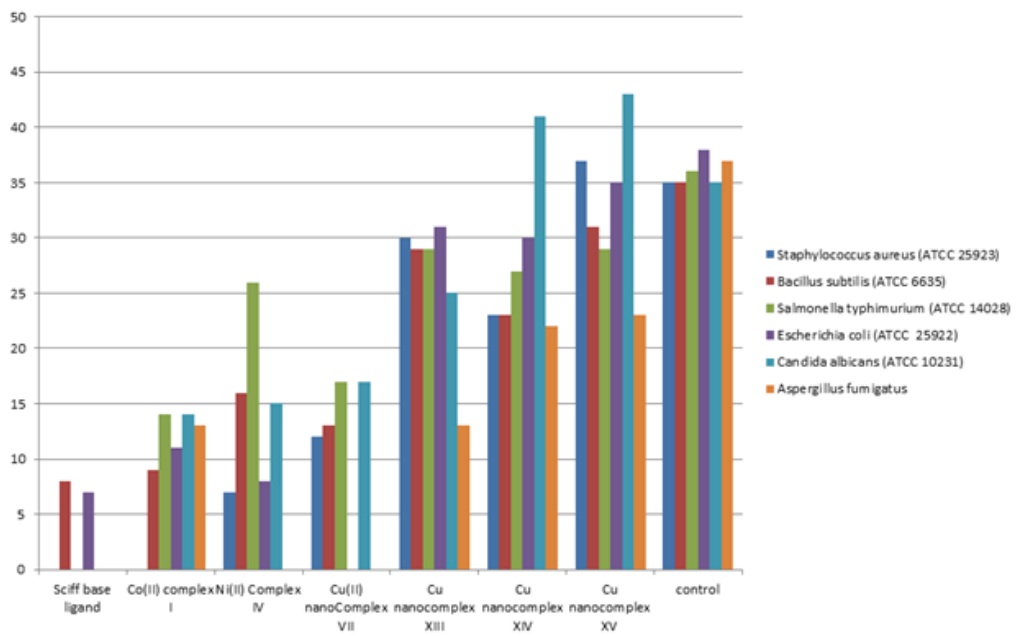


**Fig. 20** Antimicrobial and antifugi activity towards ligand and its metal complexes.

## VI. Electrical Conductivity Studies

The electrical conductivity measurements σ on the solid state for the both Cu nanocomplexes (VII and XIII) were measured in tablets form were calculated within temperature range 303-473 K. The data obtained of activation energy and electrical conductivities is listed in Table 11. The experimental data showed that increasing the electrical conductivity with increasing the temperature according the following equation:

$$\sigma = \sigma_o \exp(-E_a/K_bT)$$

Where Ea refers to activation energy of the conduction process and σo is constant value.

The plot of log σ against 1/T is found to be linear relationship with temperature range 303-473 K indicating the semi conducting behavior [52] for both Cu nanocomplexes (VII and XIII). The electrical conductivity of Cu nanocomplex XIII > Cu nanocomplex VII.

## VII. Conclusions

A new nano Copper complexes were prepared and characterized. These compounds have a great interest recently due to unique physical and chemical properties and low cost of preparation in which have great applications as antimicrobial and anticancer materials. The Cu nanocomplex used as antitumor drugs in vivo to prevent the DNA replication in the tumor cells and to suppress the cancer for further increasing. The docking study showed that metal complex is potential inhibitors of cancer causing receptors. This study has widened the scope of developing sulphaclozine compound and its metal (II) chelates as promising antitumor drugs. The newly prepared Schiff base ligand (CPHNMABS) acted as a mono-negative bidentate ligand. The metal ion coordinated through the phenolic oxygen atom and azomethine nitrogen atom. From the above obtained results of thermal and elemental analyses, conductance and magnetic moment measurements as well as different spectral studies, the proposed structures of the metal chelates under investigation can be formulated as Schemes (2 and 3)

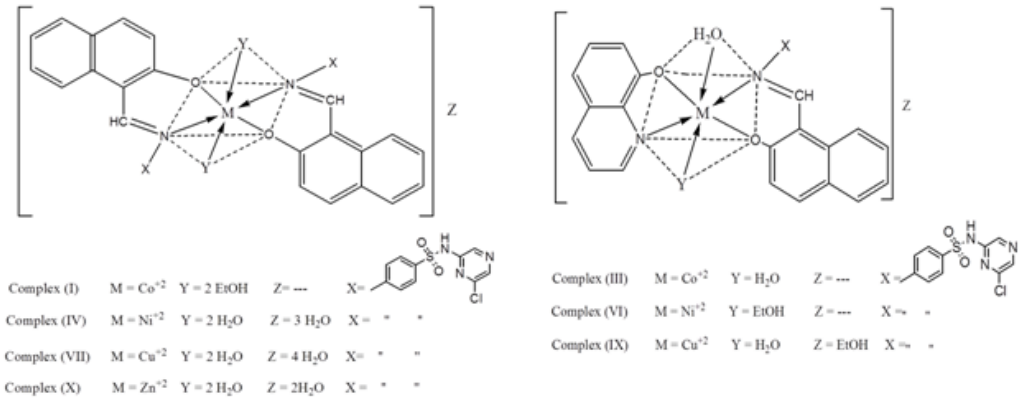


**Scheme 2** proposed structure of metal complexes.

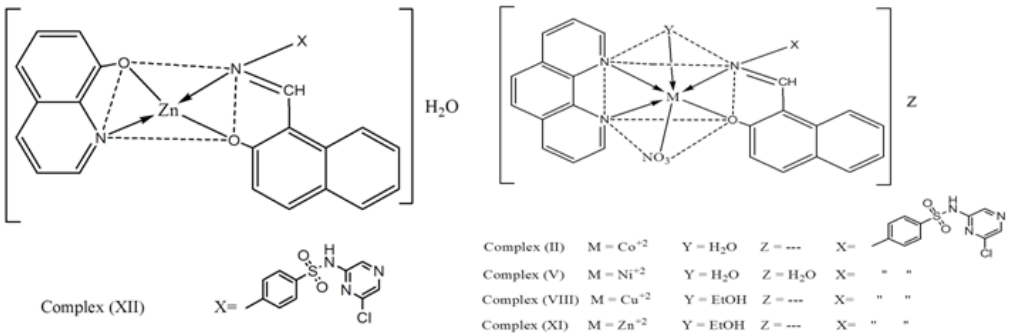


**Scheme 3** proposed structure of metal complexes.

**Table 1**. Analytical and Physical data of the metal (II) complexes of CPHNMABS (HL) ligand

| No. | Complex | Colour | m.p. (°C) | M. Wt. | Elemental analysis, found % (calcd %) | | | | | $\Omega_m$ ($ohm^{-1}$ $cm^2mol^{-1}$) |
|---|---|---|---|---|---|---|---|---|---|---|
| | | | | | % C | % H | % N | % S | % M | |
| | Schiff base ligand (CPHNMABS) | Yellow | 285 | 438.5 | 58.18 (57.46) | 2.88 (3.42) | 12.37 (12.77) | 6.93 (7.29) | ------ | ------ |
| I | $[Co(L)_2(C_2H_5OH)_2]$ | orange | > 300 | 1025.9 | 54.3 (53.8) | 3.8 (3.8) | 11.5 (10.9) | 5.83 (6.2) | 6.5 (5.74) | 8 |
| II | $[Co.(L)(Phen)(NO_3)H_2O]$ | orange | >300 | 756.4 | 54.48 (53.6) | 2.25 (2.97) | 12.38 (13.2) | 4.04 (4.3) | 8.26 (7.79) | 14.93 |
| III | [Co(L) (HQ)] | orange | >300 | 660 | 54.18 (54.5) | 4.23 (4.1) | 9.81 (10.60) | 5.82 (4.85) | 7.42 (8.7) | 4 |
| IV | $[Ni(L)_2(H_2O)_2]\ 3\ H_2O$ | green | >300 | 1023.6 | 48.97 (49.23) | 3.84 (3.71) | 10.03 (10.94) | 5.36 (6.25) | 6.63 (5.72) | 13.25 |
| V | $[Ni(L)(Phen)NO_3\ H_2O]H_2O$ | pale green | >300 | 774.2 | 51.93 (51.15) | 3.41 (3.1) | 11.68 (12.6) | 4.72 (4.1) | 7.03 (7.56) | 15.95 |
| VI | $[Ni(L)(HQ)(H_2O)\ EtOH]$ | pale green | >300 | 704.2 | 55.23 (54.5) | 3.64 (3.97) | 9.39 (9.9) | 4.03 (4.5) | 8.2 (8.3) | 8.4 |
| VII | $[Cu(L)_2.(H_2O)_2]4H_2O$ | brown | >300 | 1046.5 | 47.35 (48.16) | 3.82 (3.8) | 10.73 (10.7) | 5.9 (6.11) | 6.35 (6.07) | 13.9 |
| VIII | $[Cu(L)(Phen)NO_3\ EtOH]$ | brown | >300 | 789 | 54.9 (54.33) | 2.98 (3.6) | 11.62 (12.4) | 4.71 (4.14) | 7.62 (8.05) | 20 |
| IX | $[Cu(L)(HQ)(H_2O)_2]\ EtOH$ | brown | >300 | 727 | 52.33 (52.81) | 3.65 (4..13) | 10.47 (9.63) | 4.61 (4.4) | 8.89 (9.2) | 14 |
| X | $[Zn(L)_2(H_2O)_2]\ 2\ H_2O$ | orange | >300 | 1012 | 48.97 (49.8) | 2.92 (3.5) | 10.77 (11.04) | 5.97 (6.3) | 6.5 (6.42) | 13.5 |
| XI | $[Zn(L)(Phen)NO_3\ EtOH]$ | orange | >300 | 790.5 | 53.72 (53.13) | 3.04 (3.5) | 11.56 (12.3) | 3.5 (4.04) | 7.8 (8.2) | 19.2 |
| XII | $[Zn(L)HQ]H_2O$ | yellow | >300 | 664.5 | 54.84 (54.17) | 3.32 (3.31) | 10.34 (10.63) | 4.06 (4.8) | 9.1 (9.78) | 16.7 |

**Table 2**. Diagnostics IR bands and their assignment for CPHNMABS (HL) ligand and its metal(II) complexes

| No. | Compound or complex | IR Spectral bands ($cm^{-1}$) | | | | | | | | | |
|---|---|---|---|---|---|---|---|---|---|---|---|
| | | $\upsilon(OH)$ ($H_2O$/EtOH) | $\upsilon(OH)$ phenolic | $\upsilon(C=N)$ aliphatic | $\upsilon(C=N)$ ring | $\upsilon(SO_2)_{asm}$ | $\upsilon(SO_2)_{sym.}$ | $\rho(H_2O)$ | $\upsilon(M-O)$ | $\upsilon(M-N)$ | Other bands |
| | CPHNMABS | ------- | 3415 | 1629 | 1592 | 1154 | 1093 | ---- | ----- | ----- | ----- |
| I | $[Co(L)_2(C_2H_5OH)_2]$ | 3434 | ------ | 1617 | 1590 | 1158 | 1090 | ---- | 505 | 417 | ----- |
| II | $[Co(L)(Phen)(NO_3)H_2O]$ | 3445 | ------ | 1616 | 1589 | 1153 | 1089 | 687 | 586 | 458 | $NO_3^-$ 1385 |
| III | $[Co(L)(HQ)(H_2O)_2]$ | 3424 | ----- | 1622 | 1589 | 1157 | 1094 | 643 | 504 | 409 | ----- |
| IV | $[Ni(L)_2(H_2O)_2]\ 3\ H_2O$ | 3439 | ----- | 1617 | 1591 | 1157 | 1089 | 625 | 558 | 417 | ---- |
| V | $[Ni(L)(Phen)NO_3\ H_2O]H_2O$ | 3431 | ---- | 1618 | 1591 | 1153 | 1089 | 688 | 586 | 418 | $NO_3^-$ 1385 |
| VI | $[Ni(L)(HQ)(H_2O)\ EtOH]$ | 3444 | ----- | 1609 | 1590 | 1157 | 1090 | 625 | 505 | 470 | ----- |
| VII | $[Cu(L)_2.(H_2O)_2]\ H_2O$ | 3453 | ------ | 1617 | 1589 | 1158 | 1089 | 694 | 566 | 417 | ---- |
| VIII | $[Cu(L)(Phen)NO_3\ EtOH]$ | 3440 | ------ | 1616 | 1590 | 1157 | 1091 | ---- | 567 | 467 | $NO_3^-$ 1384 |
| IX | $[Cu(L)(HQ)]\ EtOH$ | 3446 | ----- | 1616 | 1590 | 1156 | 1091 | ---- | 566 | 417 | ----- |
| X | $[Zn(L)_2(H_2O)_2]2\ H_2O$ | 3439 | ---- | 1621 | 1591 | 1153 | 1089 | 688 | 558 | 444 | ---- |
| XI | $[Zn(L)(Phen)NO_3\ EtOH]$ | 3446 | --- | 1622 | 1591 | 1152 | 1089 | ---- | 557 | 443 | $NO_3^-$ 1384 |
| XII | $[Zn(L)8HQ]H_2O$ | 3424 | ---- | 1622 | 1591 | 1154 | 1092 | 688 | 547 | 466 | --- |

**Table 3.** $^1$HNMR signals of Schiff base ligand (CPHNMABS) and its Zn(II) complex (X)

| Compound | Chemical shifts, δ (ppm) | |
|---|---|---|
| | -N=CH- | $OH_{phenolic}$ |
| Schiff base ligand (CPHNMABS) | 8.95 | 11.95 |
| $[Zn(L)_2(H_2O)_2]2H_2O$ | 9.18 | ----- |

**Table 4**. Thermo kinetic parameters of the thermal decomposition of some complexes of the ligand (CPHNMABS)

| No. | Complex | Step | n | r | Thermodynamic activation parameters | | | | |
|---|---|---|---|---|---|---|---|---|---|
| | | | | | E* ($KJmol^{-1}$) | ΔH* ($KJmol^{-1}$) | A ($S^{-1}$) | ΔS* ($KJmol^{-1}K^{-1}$) | ΔG* ($KJmol^{-1}$) |
| I | $[Co(L)_2(C_2H_5OH)_2]$ | 1st | 0.66 | 0.998 | 0.074 | 0.341 | $5.58 \times 10^{8}$ | 0.1002 | 4.669 |
| | | 2nd | 0 | 0.998 | 0.0113 | 2.86 | $1.97 \times 10^{-5}$ | 0.173 | 57.07 |
| | | 3rd | 0.5 | 0.996 | 0.237 | 2.92 | $3.65 \times 10^{15}$ | 0.213 | 78.31 |
| | | 4th | 0.33 | 0.982 | 0.230 | 4.96 | $5.79 \times 10^{-13}$ | 0.322 | 119.15 |
| IV | $[Ni(L)_2(H_2O)_2]$ $3H_2O$ | 1st | 0.66 | 0.982 | 0.01022 | 0.721 | $1.28 \times 10^{3}$ | 0.145 | 10.47 |
| | | 2nd | 0 | 0.998 | 0.0152 | 3.2006 | $1.16 \times 10^{4}$ | 0.1594 | 58.49 |
| | | 3rd | 0.33 | 0.987 | 0.0222 | 4.39 | $6.67 \times 10^{4}$ | 0.11003 | 73.92 |
| VII | $[Cu(L)_2(H_2O)_2]$ $4H_2O$ | 1st | 0.66 | 0.990 | 0.073 | 2.211 | 2640.2 | 0.0158 | 2.144 |
| | | 2nd | 0.5 | 0.984 | 0.2615 | 2.455 | 3.429 | 0.291 | 92.716 |
| | | 3rd | 1 | 0.984 | 0.0234 | 5.48 | $1.839 \times 10^{4}$ | 0.160 | 100.65 |

**Table 5.** UV- visible spectra, $g_{eff}$ and Magnetic Moment data of the metal complexes

| No. | Complex formula | colour | Bands assignment due to d-d transition | | | Magnetic moent values (B.M) | $g_{eff}$ |
|---|---|---|---|---|---|---|---|
| | | | $\lambda_{max}$ (nm) | d-d transition | $\varepsilon_{max}$ | | |
| I | $[Co(L)_2(C_2H_5OH)_2]$ | orange | 572 | $^4T_{1g}(F) \rightarrow {}^4A_{2g}(P)$, $^4T_{1g}(F) \rightarrow {}^4T_{1g}(P)$ | 924.9 | 5.o1 | ---- |
| II | $[Co(L)(Phen)(NO_3)H_2O]$ | orange | 589 | $^4T_{1g}(F) \rightarrow {}^4A_{g}(P)$, $^4T_{1g}(F) \rightarrow {}^4T_{1g}(P)$ | 100.6 | 4.97 | ---- |
| III | $[Co(L)(HQ)(H_2O)_2]$ | orange | 582 | $^4T_{1g}(F) \rightarrow {}^4A_{2g}(P)$, $^4T_{1g}(F) \rightarrow {}^4T_{1g}(P)$ | 249.8 | 5.2 | ---- |
| IV | $[Ni(L)_2(H_2O)_2]$ $3H_2O$ | Green | 545<br>759 | $^3A_{2g} \rightarrow {}^3T_{1g}(F)$,<br>$^3A_{2g} \rightarrow {}^3T_{1g}(P)$ | 181.2<br>31.2 | 4.2 | ---- |
| V | $[Ni(L)(Phen)NO_3 H_2O]H_2O$ | Pale Green | 550<br>649 | $^3A_{2g} \rightarrow {}^3T_{1g}(F)$,<br>$^3A_{2g} \rightarrow {}^3T_{1g}(P)$ | 103.3<br>12.2 | 3.1 | ---- |
| VI | $[Ni(L)(HQ)(H_2O)EtOH]$ | Pale Green | 646<br>729 | $^3A_{2g} \rightarrow {}^3T_{1g}(F)$,<br>$^3A_{2g} \rightarrow {}^3T_{1g}(P)$ | 25.2<br>52.6 | 3.4 | ---- |
| VII | $[Cu(L)_2(H_2O)_2]$ $4H_2O$ | Brown | 542<br>704 | $^2Eg \rightarrow {}^2T_2g$ | 259.8<br>104.4 | 2.06 | 2.063 |
| VIII | $[Cu(L)(Phen)NO_3EtOH]$ | Brown | 715 | $^2Eg \rightarrow {}^2T_2g$ | 120.6 | 2.07 | 2.13 |
| IX | $[Cu(L)(HQ)(H_2O)_2]$ EtOH | Brown | 697 | $^2Eg \rightarrow {}^2T_2g$ | 95.7 | 1.8 | 2.063 |

**Table 6.** (HOMO–LUMO) energy gap (ΔE)) and the quantum chemical parameters of the ligand and its metal complexes

| Compound | HOMO | LUMO | ΔE | H | σ | χ | μ | ω | ΔNmax |
|---|---|---|---|---|---|---|---|---|---|
| HL | -5.302 | -3.314 | 1.988 | 0.994 | 1.006036 | -4.308 | 4.308 | 9.335445 | 4.334004 |
| $Co^{+2}$ complex | -3.418 | -3.083 | 0.335 | 0.1675 | 5.970149 | -3.2505 | 3.2505 | 31.53955 | 19.40597 |
| $Ni^{+2}$ complex | -3.45 | -3.3 | 0.143 | 0.0715 | 13.98601 | -3.3735 | 3.3735 | 79.58393 | 47.18182 |
| $Cu^{+2}$ complex | -3.46 | -3.31 | 0.149 | 0.0745 | 13.42282 | -3.3855 | 3.3855 | 76.92356 | 45.44295 |
| $Zn^{+2}$ complex | -3.486 | -3.346 | 0.14 | 0.07 | 14.28571 | -3.416 | 3.416 | 83.3504 | 48.8 |

**Table 7.** Bond length values of the ligand (HL) and its metal complexes

| compound | Bond | Length (A°) |
|---|---|---|
| HL | C(25) – O(26) | 1.346 |
| | N(18) – C(19) | 1.316 |
| $[Co(L)_2(C_2H_5OH)_2]$ | C(51) – O(52) | 1.419 |
| | N(33) – C(45) | 1.355 |

| | | |
|---|---|---|
| $[Ni(L)_2(H_2O)_2]4H_2O$ | C(51) – O(52) | 1.365 |
| | N(33) – C(45) | 1.338 |
| $[Cu(L)_2(H_2O)_2]4H_2O$ | C(51) – O(52) | 1.371 |
| | N(33) – C(45) | 1.361 |
| $[Zn(L)_2(H_2O)_2]2\ H_2O$ | C(51) – O(52) | 1.403 |
| | N(33) – C(45) | 1.38 |

**Table 8.** Cytotoxicity in vitro of of the Schiff base ligand and its Cu nanocomplexes on Hepatocellular Carcinoma cell line

| Compound | $IC_{50}$ µg/ml |
|---|---|
| Schiff base ligand | 31 |
| Cu nanocomplex (VII) | 13.6 |
| Cu nanocomplex (XIII) | 3.5 |
| Cu nanocomplex (XIV) | 2.46 |
| Cisplatin | 3.67 |

**Table 9.** Details of interaction of Schiff base ligand and its Cu nanocomplex with enzyme

| Compound | S (kcal/mol) | Amino acids | Interacting groups | Type of interaction |
|---|---|---|---|---|
| Shiff base ligand | -5.8251 | Glu69 | Phenyl | Arene-H |
| | | Gln92 | NH (S) | H-bond (donor) |
| | | His94 | Pyrazine | Arene-Arene |
| | | His94 | NH (S) | H-bond (acceptor) |
| Cu nanocomplex (VII) | -7.1146 | Glu69 | NH (S) | H-bond (acceptor) |
| | | Phe70 | Cl | H-bond (acceptor) |
| | | Thr199 | N (Pyrazine) | H-bond (acceptor) |
| | | Thr200 | N (Pyrazine) | H-bond (acceptor) |
| | | Phe131 | Phenyl | Arene-H |
| | | Phe131 | Phenyl (fused) | Arene-H |
| AZA | -9.6180 | | O (S) | Metal complex (Zn) |
| | | | NH (S) | Metal complex (Zn) |
| | | Leu198 | Thiadiazole | Arene-H |
| | | Leu198 | O (S) | H-bond (acceptor) |
| | | Thr199 | O (S) | H-bond (acceptor) |

**Table 10.** Antibacterial and antifungi of Schiff base ligand and its metal complexes

| | Mean* of zone diameter , nearest whole mm. | | | | | |
|---|---|---|---|---|---|---|
| | **Gram - positive bacteria** | | **Gram - negative bacteria** | | **Yeasts and Fungi**** | |
| Sample | *Staphylococcus aureus* (ATCC 25923) | *Bacillus subtilis* (ATCC 6635) | *Salmonella typhimurium* (ATCC 14028) | *Escherichia coli* (ATCC 25922) | *Candida albicans* (ATCC 10231) | *Aspergillus fumigatus* |
| Sciff base ligand | - | 8 | - | 7 | - | - |
| Co(II) complex | - | 9 | 14 | 11 | 14 | 13 |
| Ni(II) Complex | 7 | 16 | 26 | 8 | 15 | - |
| Cu(II)NanoComplex VII | 12 | 13 | 17 | - | 17 | - |
| Cu Nanocomplex XIII | 30 | 29 | 29 | 31 | 25 | 13 |
| Cu Nanocomplex XIV | 37 | 31 | 29 | 35 | 43 | 23 |
| Cu Nanocomplex XV | 23 | 23 | 27 | 30 | 41 | 22 |
| **Control #** | **35** | **35** | **36** | **38** | **35** | **37** |

**Table.11** The electrical conductivities ($\Omega^{-1}$ $cm^{-1}$) and activation energy (eV) of Cu(II) and Cu nanocomplexes

| Compounds | Cu(II) nanocomplex VII | Cu nanocomplex XIII |
|---|---|---|
| Electrical conductivities | $1.8 \times 10^{-5}$ | 6.23 |
| Activation energy | $4.3 \times 10^{-22}$ | $1.5 \times 10^{-19}$ |

## Reference


[1]. H. Rehman, A. Qadir, HA Shad, Z I Khan. Med. Chem **2017** 7:252.
[2]. Y. Kwon, J. Song, H. Lee, E-Y. Kim, K. Lee, S. K. Lee, S. Kim, J. Med. Chem. **2015**, 58, 7749.
[3]. G. B. Bagihalli, P. G. Avaji, S. A. Patil, P. S. Badami, Eur. J. Med. Chem. **2008**, 43, 2639.
[4]. G. Valarmathy, R. Renganathan, J. Mol. Struct. **2020**, 1199, 127029
[5]. K. Siddappa, Nabiya Sultana Mayana, Int J Pharm Bio Sci. **2014**, 5, 162-174
[6]. S. Mondal, T. K. Mondal, Y. Rajesh, M. Mandal, C. Sinha, Polyhedron **151** (**2018**). **344**-354.
[7]. C. M. Sharaby, M. F. Amine, A. A. Hamed, J. Mol. Struct., **2017**, 1134, 208-216
[8]. M. Aidi, H. Keypour, A. Shooshtari, M. Bayat, L. Hosseinzadeh, H. A. Rudbari, R. W. Gable, Inorg. Chim. Acta **2019** ,490, 294.
[9]. A. Agudo-López, E. Prieto-García, J. Alemán, C. Pérez, C. V. Díaz- García, L. Parrilla-Rubio, S. Cabrera, C. Navarro-Ranninger, H. Cortés-Funes, J. A. López-Martín, M. T. Agulló-Ortuño, Mol. Cancer **2017**, 16(1), 45.
[10]. K. G. Samper, S. C. Marker, P. Bayón, S. N. MacMillan, I. Keresztes, O. Palacios, J. J. Wilson, J. Inorg. Biochem. **2017**, 174, 102-110
[11]. M. Sevim, T. Sener, O. Metin, Inter J. Hydrogen energy **2015**, 40, 10876 -10882
[12]. L. Guerrini, R. A. Alvarez-Pueble, N. Pazos-Perez, Materials **2018**, 11, 1154.
[13]. A. I. Vogel, A Text Book of Quantitative Inorganic Analysis, 3rd ed., Longman ELBS, London **1968**.
[14]. T. M.A. Ismail, H. M.A Soliman, S. M. Abu-El-Wafa, D. F. Sallam, J. Chem. Bio. Phy. Sci. Sec. A, **2016**, 6, 751.
[15]. T. M. Ismail, M. A. EL Ghamry, S. M. Abu-El-Wafa, D. F. Sallam, Modern Chemistry, **2015**, 3, 18.
[16]. B. Delley. Hardness conserving semilocal pseudopotentials.Phys Rev B **2002**; 65:85403–9.
[17]. J. Z. Charmm, M. Schaefer, B. Tidor, R. M.Venable, H. L. Woodcock, X. Wu, Modeling and Simulation Solutions for Chemicals and Materials Research, Accelrys Materials Studio (Version 5.0). San Diego, USA: Accelrys Software Inc.; **2009** <http://www.accelrys.com>.
[18]. T. Mosmann, J. Immunol. Methods **1983**, 65, 55-63
[19]. S. M. Gomha, S. M. Riyadh , E. A. Mahmmoud, M. M. Eaasser, Heterocycles **2015**, 91, 1227-1243
[20]. J. Tota, S. Battu, Inter. J. Res. Pharm. Chem. IJRPC **2018**, 8, 258-267
[21]. F. arjmand, I. yousuf, J. Organometal. Chem. **2013**, 743, 55-62
[22]. A. A. Athawale, P. P Kater, M. Kumar, M. B. Majumdar, Mater. Chem. Phys. **2005**, 91, 507-512
[23]. M. F. Zayed, W. H. Eisa, A. A. Shabaka, Spectrochim. Acta A **2012**, 96, 423-428
[24]. M. F. Zayed, W. H. Eisa, A. M. Hezma, J. appl. Spectroscopy **2017**, 83, 1046-1050
[25]. T. Manjuraj, G. Krishnamurthy, Y. D. Bodke, H. S. B. Naik, H. S. A. Kumar, J. Mol. Struct. **2018**, 1171, 481-487
[26]. T. Manjuraj, G. Krishnamurthy, D. B. Yadav, H. S. B. Naik, J. Mol. Struct. **2017**, 1148, 231-237
[27]. T. M. A. Ismail, A. A. Saleh, M. A. El Ghamry, Spectrochim. Acta A **2012**, 86, 276-288
[28]. M. Shebl, S.M.E. Khalil, Monatsh Chem, **2015**, 146, 15-33
[29]. K. Nakamoto, Infrared and Raman Spectra of Inorganic and Coordination Compounds, 4th ed., JohnWiley, Nature. 68 (**1964**) 201.
[30]. H.F. El-Shafiy, M. Shebl, J. Mol. Struct. **2019**, 1194, 187.
[31]. H.F. El-Shafiy, M. Shebl, J. Mol. Struct. **2018**, 1156, 403.
[32]. M. Shebl, Spectrochim. Acta A **2014**,117, 127.
[33]. A. W. Coats, J. P. Redfern. Metal Chem. **2001**, 26, 532.
[34]. C. R. Vinodkumar, M. K. Muraleedharan Nair, P. K. Radhakrishnan, J. Therm. Anal. Cal. **2000**, 61, 143.
[35]. A. L Sharma, I. O, singh, H. R. singh, R. M Kadam, M. K Bhide, M. D. Snstry, Transit and Sons, New York, **1986**.
[36]. D. N. Abdeen, M. El Hachach, M. Koc, M. A. Atieh, Materials **2019**, 12, 210.
[37]. M. Shebl, J. Coord. Chem. **2016**, 69, 199.
[38]. O. f. Ozturk, A. Cansiz, M. Koparir, Transit Metal Chem. **2007**, 32, 224.
[39]. A. A. Saleh, J. Coord. Chem. **2005**, 58, 255.
[40]. M. Mashaly, T. M. Ismail, S. B. E. L. Maraghy, H. A. Habib, J. Coord. Chem. **2004**, 57, 1099.
[41]. M. Shebl, Spectrochim. Acta A **2009**, 73, 313.
[42]. A. B. P. Lever, Inorganic Electronic Spectroscopy, Elsevier, New York, (1984).
[43]. T. M. A. Ismail, J. Coord. **2005**, 58,141.
[44]. M. Shebl, J. Mol. Struct. **2017**, 1128, 79.
[45]. T. A. Yousef, G. M. Abu El-Reash, R. M. El Morshedy, Polyhedron **2012**, 45, 71.
[46]. J. Fang, J. Li, J. Mol. Struct. **2002**,593, 179.
[47]. T. A. Yousef, O. K. Alduaij, S. F. Ahmed, G. M. Abu El-Reash, O. A. El-Gammal, J. Mol. Struct. **2016**, 1125, 788.
[48]. N. Raman, A. Sakthivel, K. Rajasekaran, J. Coord. Chem. **2009**, 6 1661.
[49]. A. Kulkarni, S. A Patil, P. S. Badami, Eur. J. Med. Chem. **2009**, 44, 2904
[50]. S. Belaid, A. Landreau, S. Djebbar, O. Benali-Baitich, G. Bouet, J. P. Bouchara, J. Inorg. Biochem. **2008,** 55, 102.
[51]. S. Amer, N. El-Wakiel, H. El-Ghamry, J. Mol. Struct. **2013**, 1049, 326.
[52]. M. S. Refat, I. M. El-Deen, M. A. Zein, A. A. Adam, M. I. Kobeas, Int. J. Electrochem. Sci. **2013**, 8, 9894.